

Energy Dependence of Cumulants of Net-Kaon Multiplicity Distributions at RHIC

PAs (alphabetically):

Feng Liu, Xiaofeng Luo, Bedanga Mohanty, Jochen Thäder, Ji Xu, Nu Xu

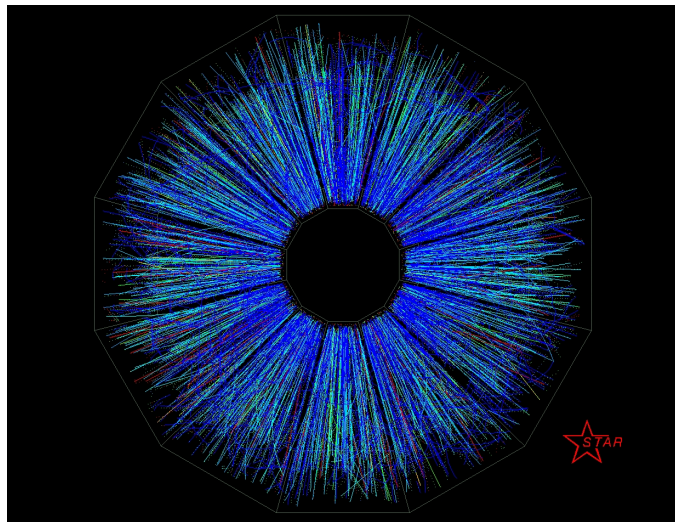
2016

Abstract

One of the main goals of the RHIC Beam Energy Scan (BES) program is to search for the QCD critical point. By varying the colliding energy, we can access different regions (T , μ_B) on the QCD phase diagram. Fluctuations of conserved quantities such as baryon number (B), charge number (Q), and strangeness number (S), are sensitive to the correlation length and can be used to probe non-gaussian fluctuations near the critical point. Experimentally, higher moments of the multiplicity distributions have been used to search for the QCD critical point in heavy-ion collisions.

We present the first STAR measurement of the higher moments of the mid-rapidity ($|y| < 0.5$) net-kaon multiplicity distributions in Au+Au collisions at $\sqrt{s_{NN}} = 7.7, 11.5, 14.5, 19.6, 27, 39, 62.4$, and 200 GeV. The data were collected during the first phase of the RHIC BES program by the STAR experiment. Centrality and energy dependence of cumulants up to the fourth order as well as their ratios are shown. Furthermore, the comparisons with baseline calculations (Poisson, Negative Binomial) and non-critical point models (UrQMD) have been discussed as well.

Webpage: http://www.star.bnl.gov/protected/bulkcorr/xuj/Netkaon_Webpage/PaperProposal.dwt



Contents

1	Introduction	3
2	Moments method in heavy ion collision	3
3	Particle selection and identification	4
3.1	Data set	4
3.2	Event Selection	4
3.3	Track Quality Cuts	5
3.4	Kaon Identification	7
3.5	Purity of kaon	8
4	Centrality Definition	9
5	Net-Kaon Distributions	12
6	The volume fluctuation effect	12
6.1	The centrality bin width effect (CBWE) and correction	13
6.2	The centrality resolution effect (CRE)	14
7	Efficiency correction and statistical error estimation	14
8	Systematic error estimation	18
9	Baselines for the higher moments	21
9.1	Poisson expectation	21
9.2	Negative Binomial Distribution	21
9.3	UrQMD simulation	22
10	Results	22
11	Summary and Outlook	27

1 Introduction

Fluctuations of conserved quantities, such as net-baryon (ΔN_B), net-charge (ΔN_Q) and net-strangeness (ΔN_S), have long been predicted to be sensitive to the QCD phase transition and the QCD critical point [1, 2, 3]. Experimentally, one can measure various order moments (variance (σ^2), skewness (S), and kurtosis (κ)) of the conserved quantity distributions in heavy-ion collisions. These moments are sensitive to the correlation length (ξ) of the hot dense matter created in the initial collision and are also connected to the thermodynamic susceptibilities computed with Lattice QCD [4, 5] and in the Hadron Resonance Gas (HRG) model [6, 7]. It has been proposed that variance, skewness, and kurtosis is related to different powers of the correlation length as ξ^2 , $\xi^{4.5}$, and ξ^7 [1], respectively. Furthermore, the n^{th} order susceptibility $\chi^{(n)}$ are related to cumulant as $\chi^{(n)} = C_n/VT^3$, where V, T are the volume and temperature of the system, and C_n is the n^{th} order cumulant of a multiplicity distribution. In order to compare with theoretical calculations, cumulant ratios ($S\sigma = C_3/C_2$, $\kappa\sigma^2 = C_4/C_2$) are constructed to cancel the volume (VT^3). Thus, those cumulant ratios are also directly related to the ratios of various order susceptibilities as $C_4/C_2 = \chi_i^{(4)}/\chi_i^{(2)}$ and $C_3/C_2 = \chi_i^{(3)}/\chi_i^{(2)}$, where i indicates the conserved quantity.

Experimentally, it is very hard to measure the net-baryon (ΔN_B) and the net-strangeness (ΔN_S) distributions, so we use net-proton (ΔN_P) and net-kaon (ΔN_K) as proxies respectively. In this work, we report recent efficiency-corrected cumulants and cumulant ratios of the net-kaon (ΔN_K) multiplicity distributions in Au+Au collisions at $\sqrt{s_{NN}} = 7.7, 11.5, 14.5, 19.6, 27, 39, 62.4$, and 200 GeV collected in 2010, 2011, and 2014 by STAR at RHIC.

2 Moments method in heavy ion collision

In statistics, the distribution function can be characterized by the various moments, such as mean (M), variance (σ^2), skewness (S), kurtosis (κ). Before introducing the above moments used in our analysis, we would like to define cumulants, which are alternative approach compared to moments to characterize a distribution.

In the moments analysis, we use N to represent the net-kaon($N_{K^+} - N_{K^-}$) number in one event. The average value over whole event ensemble is denoted by $\langle N \rangle$. We use $\delta N = N - \langle N \rangle$ to denote the deviation of N from its mean value. Then the various order cumulants of event-by-event distributions of a variable N are defined as:

$$C_{1,N} = \langle N \rangle \quad (1)$$

$$C_{2,N} = \langle (\delta N)^2 \rangle \quad (2)$$

$$C_{3,N} = \langle (\delta N)^3 \rangle \quad (3)$$

$$C_{4,N} = \langle (\delta N)^4 \rangle - 3 \langle (\delta N)^2 \rangle \quad (4)$$

Once we have the definition of cumulants, various moments can be denotes as:

$$M = C_{1,N}, \sigma^2 = C_{2,N}, S = \frac{C_{3,N}}{(C_{2,N})^{\frac{3}{2}}}, \kappa = \frac{C_{4,N}}{(C_{2,N})^2} \quad (5)$$

In addition, the moments product $\kappa\sigma^2$ and $S\sigma$ can be expressed in term of cumulant ratio:

$$\kappa\sigma^2 = \frac{C_{4,N}}{C_{2,N}}, S\sigma = \frac{C_{3,N}}{C_{2,N}} \quad (6)$$

With above definitions, we can calculate various cumulants and ratios of cumulants for the measured event-by-event net-kaon multiplicity distributions.

3 Particle selection and identification

3.1 Data set

In the first phase of the Beam Energy Scan (BES) program at RHIC, eight beam energies have already been analyzed from $\sqrt{s_{NN}} = 7.7\text{GeV}$ to 200GeV . The details of the BES-I program are listed in table 1.

$\sqrt{s_{NN}}(\text{GeV})$	Statistics(M)	Year	$\mu_B(\text{MeV})$	T(MeV)	μ_B/T
7.7	~ 4	2010	420	140	3.020
11.5	~ 12	2010	315	152	2.084
14.5	~ 20	2014	266	156	1.705
19.6	~ 36	2011	205	160	1.287
27	~ 70	2011	155	163	0.961
39	~ 130	2010	115	164	0.684
62.4	~ 67	2010	70	165	0.439
200	~ 350	2010	20	166	0.142

Table 1: Data set of Beam Energy Scan Phase I, including the statistics, the year of the production, and the corresponding baryon chemical potential and temperature which is extracted from Hadron Resonance Gas (HRG) model [8].

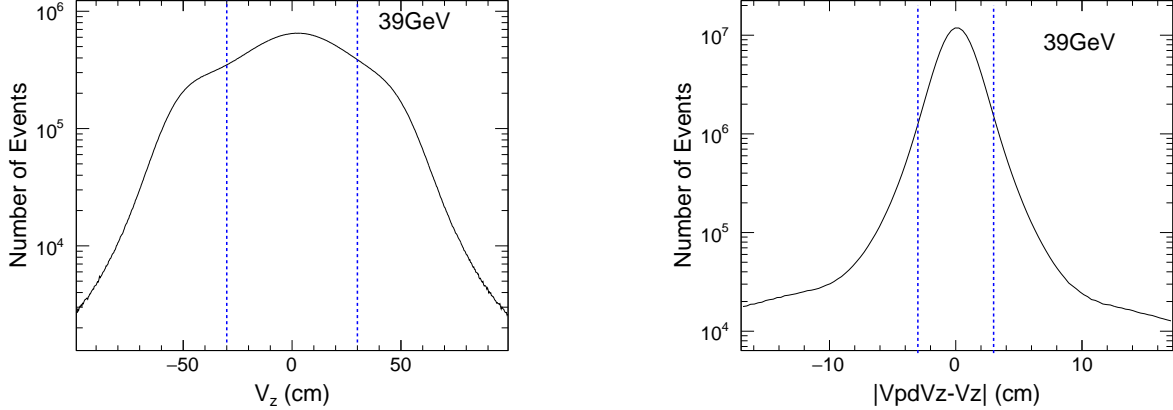
All the data are taken with mini-bias trigger. Table 2 shows the trigger information used in all the 8 energies for the analysis.

$\sqrt{s_{NN}}(\text{GeV})$	Production	Trigger Name	TriggerID
7.7	AuAu7_Production	P10ih	290001, 290004
11.5	AuAu11_Production	P10ih	310004, 310014
14.5	production_15GeV_2014	P14ii	440015, 440016
19.6	AuAu19_Production	P11ik	340001, 340011, 340021
27	AuAu27_Production_2011	P11id	360001
39	AuAu39_Production	P10ik	280001
62.4	AuAu62_Production	P10id	270001, 270011, 270021
200	AuAu200_production	P1o1k	260001, 260011, 260021, 260031

Table 2: Trigger ID of mini-bias trigger for Beam Energy Scan phase I

3.2 Event Selection

Events with a reconstructed primary vertex position in the fiducial region $|V_z| < 30 \text{ cm}$ ($< 50 \text{ cm}$ for 7.7GeV) and $|v_r| < 2\text{cm}$ ($< 1\text{cm}$ for 14.5GeV) were considered. At higher energies, the luminosity is always higher, which means that particles from a previous event could still be traversing the TPC when a new event triggered the detector to begin reading out data, a problem called pile-up. In this case, $|VpdVz - Vz| < 3$ is applied to suppress the pile-up events at $39, 62.4$, and 200GeV .

Figure 1: v_z distribution for Au+Au 39GeVFigure 2: $|V_{pd}V_z - V_z|$ distribution for Au+Au 39GeV

All the event cuts are listed in the table 3. From figure 1 to figure 4, we presented the distributions for $|V_z|$, $|V_{pd}V_z - V_z|$, V_x vs V_y , and V_r at $\sqrt{s_{NN}} = 39$ GeV, respectively. The event cuts for all the 8 energies are listed in table 3.

$\sqrt{s_{NN}}$ (GeV)	$ V_z $	$ V_r $	$ V_{pd}V_z - V_z $	TofMult
7.7	50	2	Nan	2
11.5	30	2	Nan	2
14.5	30	1	Nan	2
19.6	30	2	Nan	2
27	30	2	Nan	2
39	30	2	3	2
62.4	30	2	3	2
200	30	2	3	2

Table 3: Event selection cuts used in BESI energies.

To ensure the quality of our data, run by run study of many variables have already performed to remove the bad runs for every energy. For instance, the run by run QA for average Refmult, dca, p_T , η , ϕ at 19.6 GeV and remove the outlier runs beyond $+/-3\sigma$. The Data QA for 14.5GeV is shown as figure 5 and the details can be find in [xiaofeng/Moments_14.5GeV_20150211.pdf](#). The bad runs list for 14.5GeV can be found in: [newbadrunlist.txt](#). Bad runs list for other energies can be found in: [bad_runs_3sig.txt](#)

3.3 Track Quality Cuts

Track Selection cuts for all energies are listed in table 4. In order to reduce the contamination from secondary charged particles, only primary particles have been selected, requiring a distance of closest approach (DCA) to the primary vertex of less than 1 cm. Tracks must have at least 15 points (nFitPoints) used in track fitting out of maximum of 45 hits possible in the TPC. The minimum number of points used to derive dE/dx values is limited to 5. To prevent multiple counting of split tracks, at least 52% of the total possible fit points are required (nHitsFit/NFitPoss). All the

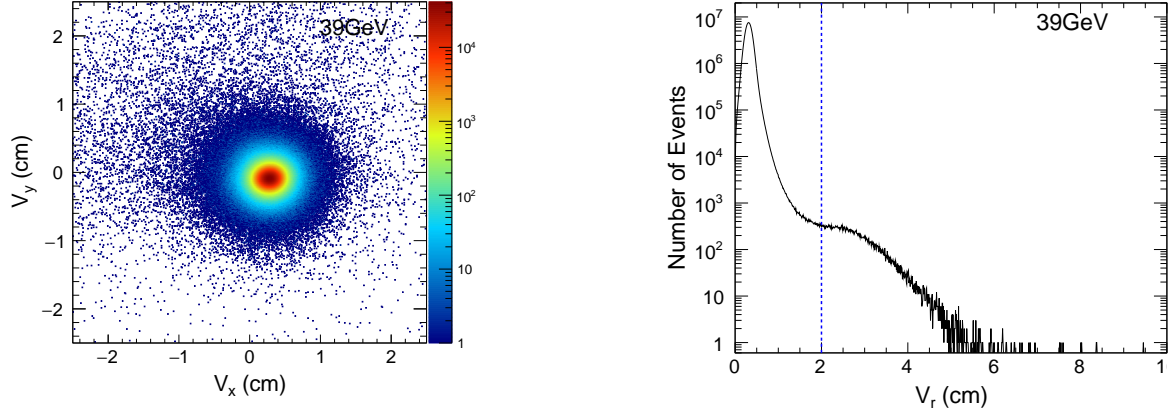


Figure 3: V_x vs V_y distribution for Au+Au 39GeV

Figure 4: V_r distribution for Au+Au 39GeV

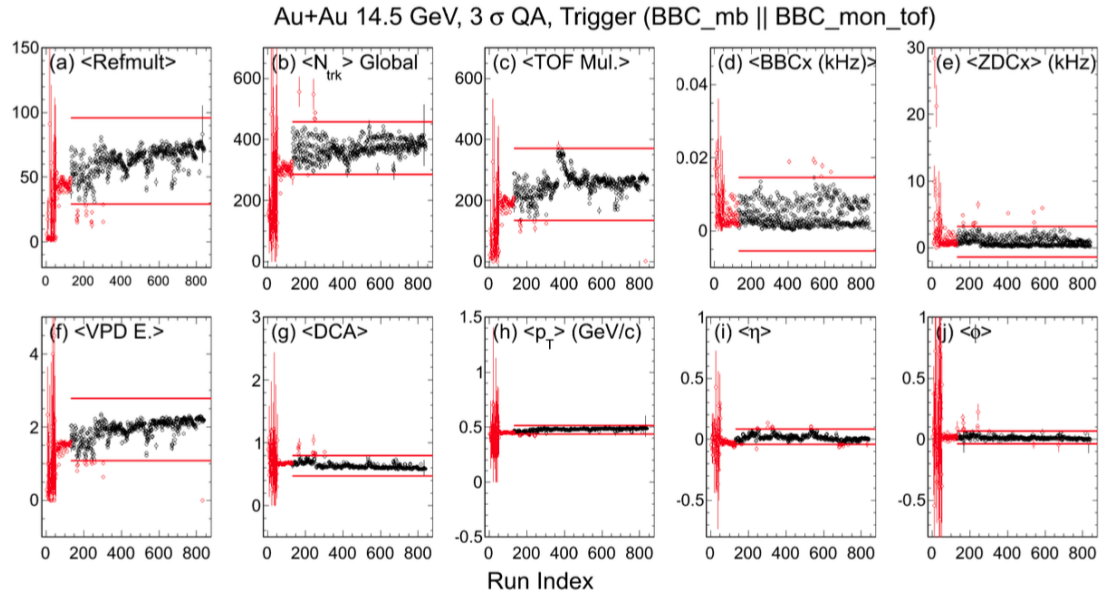


Figure 5: Data QA at Au+Au $\sqrt{s_{NN}} = 14.5$ GeV.

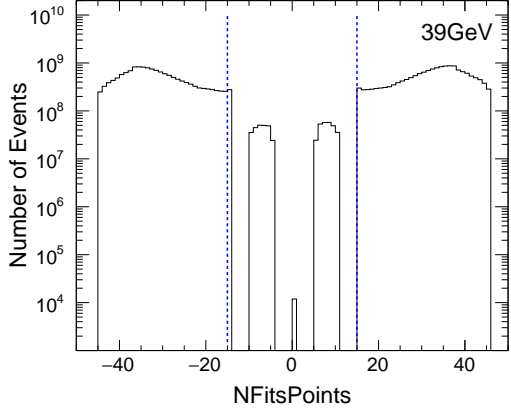


Figure 6: NFitsPoints distribution for Au+Au 39GeV

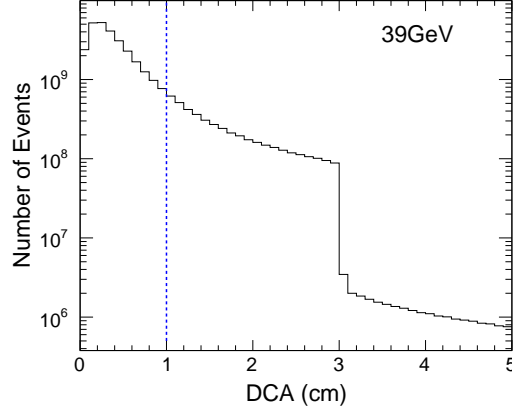


Figure 7: DCA Distribution for Au+Au 39GeV

tracks are taken within mid-rapidity $|y| < 0.5$, and transverse momentum range $0.2 < p_T < 1.6$ (GeV/c). These cuts are same for all the 8 energies.

Transverse Momentum (p_T)	$0.2 < p_T < 1.6$ (GeV)
Rapidity ($ y $)	< 0.5
NfitPoints	> 15
nhitdedx	> 5
gDCA	< 1
nHitsFit/NFitPoss	> 0.52

Table 4: Track quality cuts used in BESI energies.

3.4 Kaon Identification

The STAR (Solenoidal Tracker At RHIC) detector [9] at BNL has a large uniform acceptance at mid-rapidity and excellent particle identification capabilities. Energy loss (dE/dx) in the Time Projection Chamber [10] and mass-squared (m^2) from the Time-Of-Flight [11, 12] detector are used to identify kaons.

The left panel of figure 8 show the ionization energy loss distributions as a function of particle momentum, which are measured by STAR TPC and can be used to identify charged particles. The energy resolution of the ionization energy loss measurement σ_E is the standard deviation of the gaussian distribution for the truncated mean values and is proportional to the energy deposit δE . The relative energy resolution for energy loss of STAR TPC is about $\sigma_E/E = 7.5\%$. To ensure good gaussian distributions, another variable is constructed to identify particles in the STAR experiment, which is defined as:

$$Z = \frac{\log[(dE/dx)_{measure}/(dE/dx)_{theory}]}{\sigma_E} \quad (7)$$

where $(dE/dx)_{theory}$ is the Bethe-Bloch [13] expectation for the given particle type (eg. π, K, p),

it is parametrized as:

$$\langle dE/dx \rangle_{BB} = A(1 + \frac{m^2}{p_{mag}^2}) \quad (8)$$

where m is the particle rest mass and p_{mag} is the particle momentum magnitude. This parametrization is found to describe the data well, with the normalization factor A determined from data. The expected value of z for the particle in study is around 0. In our higher moments of net-kaon distribution analysis, we select kaons and anti-kaons event-by-event by using cut $|Z_K| < 2$ within transverse momenta $0.2 < pT < 1.6(\text{GeV}/c)$ and mid-rapidity $|y| < 0.5$.

Another detector used to identify particles in our analysis is the Time of flight detector (TOF), which measures the flight time of a particle from the primary vertex of the collision. Once the time of flight and path length information are obtained, we can directly calculate the velocity of the particles and their mass.

$$\beta = \frac{v}{c} = \frac{L}{ct} \quad (9)$$

$$m^2 = (\frac{1}{\beta^2})xp = (\frac{c^2t^2}{L^2} - 1)xp \quad (10)$$

The right panel of figure 8 shows the mass square as a function of rigidity for Au+Au collision at $\sqrt{s_{NN}} = 14.5 \text{ GeV}$. In this analysis, we use mass square cut $0.15 < m^2 < 0.4(\text{GeV}^2/c^4)$ to select proton and anti-proton within the p_T range $0.4 < pT < 1.6(\text{GeV}/c)$.

$0.2 < p_T < 0.4 \text{ (GeV)}$	$0.4 < p_T < 1.6 \text{ (GeV)}$
TPC	TPC + TOF
$ Z_K < 2$	$ Z_K < 2, 0.15 < m^2 < 0.4$

Table 5: Kaon identification cuts used in different transverse momentum range.

The K^+ (K^-) for net-kaon are measured at mid-rapidity ($|y| < 0.5$) within the transverse momentum $0.2 < p_T < 1.6 \text{ (GeV}/c)$. In order to maximize the purity and efficiency of kaons, we split the transverse momentum range into two intervals: the lower p_T range ($0.2 < p_T < 0.4 \text{ GeV}/c$) with TPC only, and the higher p_T range ($0.4 < p_T < 1.6 \text{ GeV}/c$) with both TPC and TOF. Figure ?? shows the kaon accepted phase space within STAR TPC and TOF. The kaon included in the blue box are used in the moment analysis.

3.5 Purity of kaon

In the lower p_T range ($0.2 < p_T < 0.4 \text{ GeV}/c$), $|n\sigma_K| < 2$ from TPC de/dx are applied. In the higher p_T range ($0.4 < p_T < 1.6 \text{ GeV}/c$), additional cut $0.15 < m^2 < 0.4$ from TOF are applied. Figure 9 shows the $n\sigma_K$ distribution from TPC de/dx at 14.5GeV, the lines are fitted by Gaussian. Figure 10 shows the mass square distributions from TOF, the lines are fitted by Student's t-distribution. The student's t-distribution can be expressed as:

$$f(t) = \frac{\Gamma(\frac{\nu+1}{2})}{\sqrt{\nu\pi}\Gamma(\frac{\nu}{2})}(1 + \frac{t^2}{\nu})^{-\frac{\nu+1}{2}} \quad (11)$$

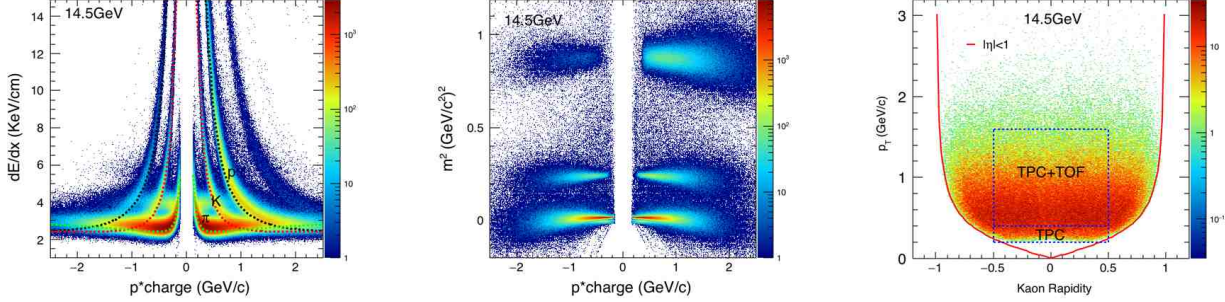


Figure 8: Left panel: The dE/dx of tracks plotted as function of rigidity (charge*momentum) for Au+Au 14.5GeV. The dashed lines in the figure are expectation line from bethe-bloch formula. Middle: Mass square vs. rigidity distributions at Au+Au 14.5 GeV. Right: The kaon accepted phase space within STAR TPC and TOF. The kaon distributed in the blue box are used in the moment analysis.

Once we have the fit parameters, we can get the purity of kaons in different p_T bins shown as figure 11. At lower momentum range ($0.2 < p_T < 0.4$ GeV/c), the purity is lower than high momentum range ($0.4 < p_T < 1.6$ GeV/c). The purity decrease with the momentum increase at higher momentum range. The purity for other energies can be found in: [Purity_check.pdf](#).

4 Centrality Definition

The centrality of nucleus-nucleus collisions is an important parameter in heavy ion collision physics. It can be defined by several different parameters, such as impact parameter b , the number of nucleons that participate, N_{part} and the number of binary collisions, N_{coll} . Unfortunately, those geometry observables can not be directly measured and must be deduced from a combination of experimentally measured quantities and Monte-Carlo simulations. This usually is done by a purely geometric model, the so called Glauber model [14].

In the STAR experiment, the efficiency-uncorrected charged particle multiplicity, which is also called reference multiplicity measured by the Time Projection Chamber (TPC) and Time of Flight (TOF) combined with Glauber model simulations is used for centrality determination. In our analysis, the definition of reference multiplicity is defined as figure 12. It consists most of pions and protons. We call this definition refmult4. The reason that we only use the multiplicity of charged kaons and pions to define the centrality in Au+Au collisions is to avoid the effect of auto-correlation between kaons/anti-kaons involved in our moment analysis and in the centrality definition.

Figure 13 shows the normalized reference multiplicity 4 distributions for Au+Au collisions from $\sqrt{s_{NN}} = 7.7$ GeV to 200GeV, which are used for centrality definition in net-kaon moments analysis. Red lines come from the fittings from Glauber MC simulation. We can calculate the reference multiplicity and determine the centrality classes with Glauber model simulations, in which the average geometrical parameters (N_{part} and N_{coll}) for each centrality bin can be also calculated. The blue bands indicate the 0-5% most central collisions, which is defined by binning the distribution on the basis of the fraction of the total integral. The detailed study of centrality can be found in : [RefMult4.pdf](#).

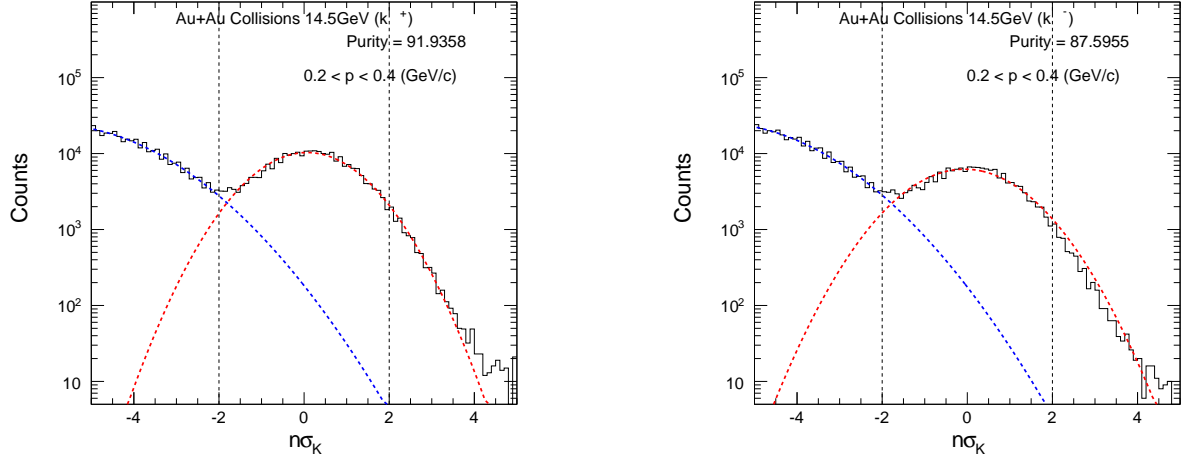


Figure 9: Left: $n\sigma_{kaon}$ distribution from TPC de/dx for K^+ at 14.5 GeV. Right: $n\sigma_{kaon}$ distribution from TPC de/dx for K^- at 14.5 GeV. Blue and red lines are fitted by gaussian.

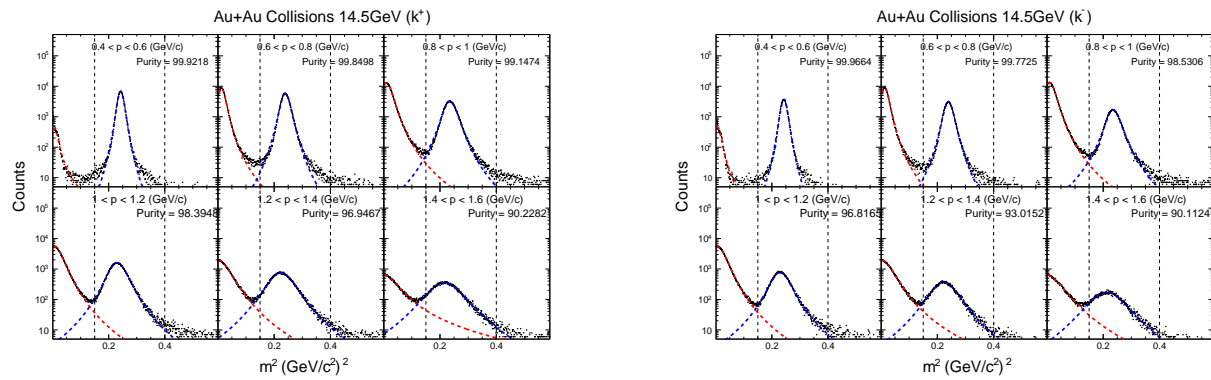


Figure 10: Left: mass square distribution from TOF for K^+ at 14.5 GeV. Right: mass square distribution from TOF for K^- at 14.5 GeV. The blue and red lines are fitted by Student's t-distribution.

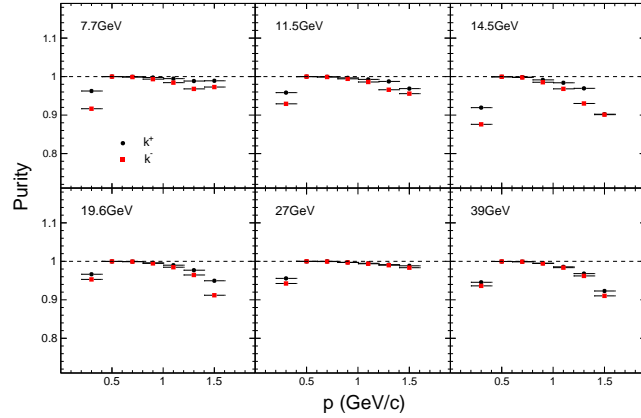


Figure 11: Kaon purity plotted as the function of momentum at Au+Au $\sqrt{s_{NN}} = 7.7, 11.5, 14.5, 19.6, 27$ and 39GeV .

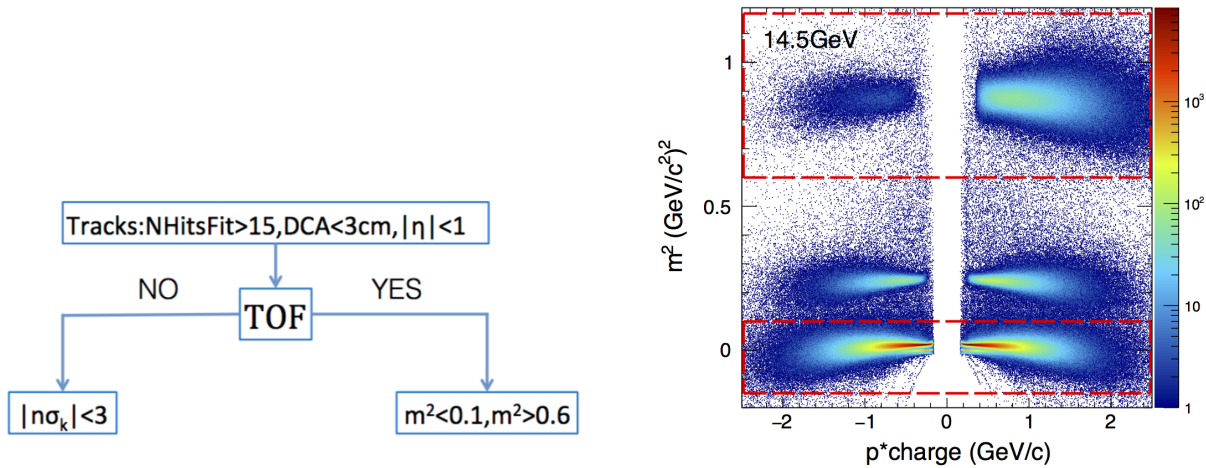


Figure 12: Left: Cuts used in the definition of reference multiplicity for centrality determination. Right: Mass square vs. rigidity to illustrate that reference multiplicity 4 is consist most of protons and pions.

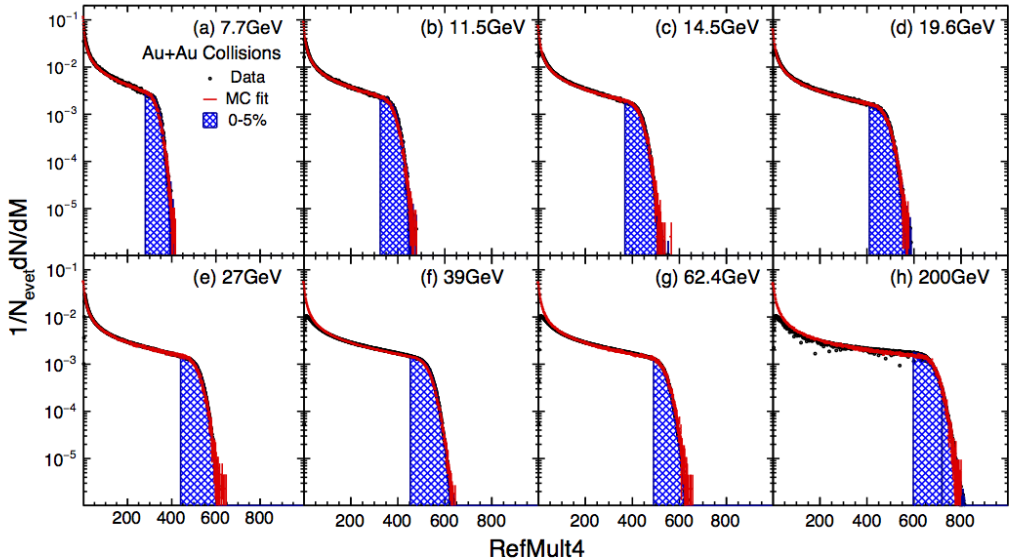


Figure 13: Normalized reference multiplicity 4 distributions for Au+Au collisions from $\sqrt{s_{NN}} = 7.7$ GeV to 200GeV, which are used for centrality definition in net-kaon moments analysis. Red lines come from the fittings from Glauber MC simulation.

5 Net-Kaon Distributions

After the kaon identification and centrality is done , we can get the event-by-event net-kaon distributions. Event-by-event net-proton multiplicity distributions for various colliding energies are measured within $0.4 < p_T < 0.8$ GeV/c and $|y| < 0.5$. The uncorrected raw event-by-event net-kaon multiplicity distributions for 0-5% top central, 30-40% central, and 70-80% peripheral collisions are shown at figure 14. We can see that most central collisions have a wider distribution compared with peripheral collisions. The peak of the net-kaon distributions shift slightly towards the positive direction as the energy decreases. These distributions are raw distributions, and some effects need to be addressed to get final moments/cumulants. These effects include auto-correlation effects, effects of volume fluctuations, and finite detector efficiency [15, 16, 17].

6 The volume fluctuation effect

In heavy-ion collisions, the collision centrality and/or initial collision geometry of two nuclei with finite volume is estimated by comparing the particle multiplicities with the Glauber simulation [14] and cannot be measured directly. This drawback in general can cause two effects in the moment analysis of particle multiplicity distributions within a finite centrality bin. One is the so-called CBWE [18], which is caused by volume variation within a finite centrality bin size and the other is the CRE, which is caused by the initial volume fluctuations [19].

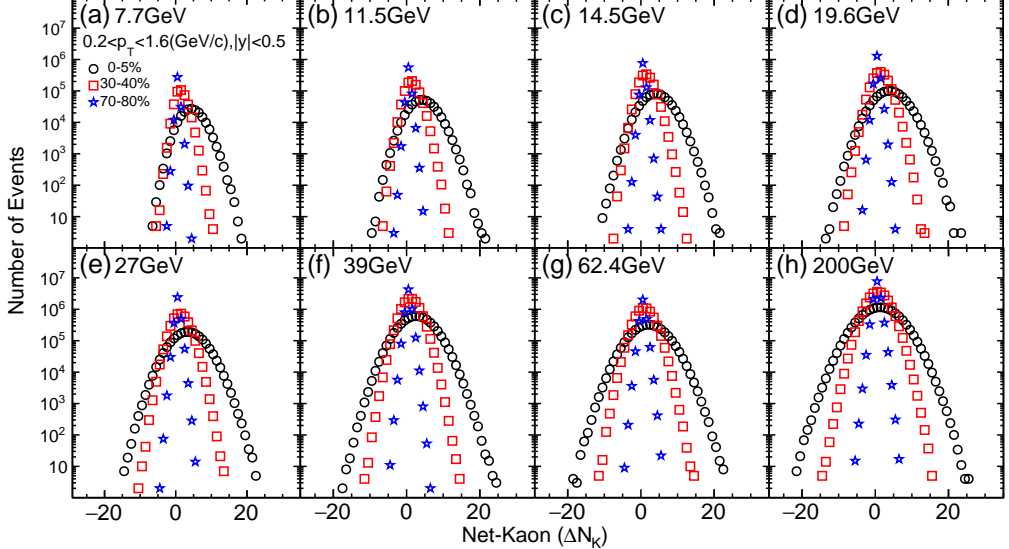


Figure 14: Uncorrected raw event-by-event net-kaon multiplicity distributions for Au+Au collisions at various $\sqrt{s_{NN}}$ for 0-5% top central (black circles), 30-40% central (red squares), and 70-80% peripheral collisions (blue stars).

6.1 The centrality bin width effect (CBWE) and correction

Generally, we report the results for a wider centrality bin, such as 0-5% and 5-10%, for better statistical accuracy. But before calculating various moments of particle number distributions for one wide centrality bin, such as 0-5%, 5-10%, we should consider the so-called CBWE arising from the impact parameter (or volume) variations due to the finite centrality bin. This effect must be eliminated, as an artificial centrality dependence could be introduced due to finite centrality bin width.

To eliminate the CBWE, we have applied a technique called centrality bin width correction (CBWC), to calculate the various moments of particle number distributions in one wide centrality bin. These formulas are:

$$\sigma = \frac{\sum_r n_r \sigma_r}{\sum_r n_r} = \sum_r \omega_r \sigma_r \quad (12)$$

$$\sigma = \frac{\sum_r n_r S_r}{\sum_r n_r} = \sum_r \omega_r S_r \quad (13)$$

$$\sigma = \frac{\sum_r n_r \kappa_r}{\sum_r n_r} = \sum_r \omega_r \kappa_r \quad (14)$$

where n_r is the number of events in the r th multiplicity for centrality determination, and σ_r , S_r and κ_r represent the standard deviation, skewness and kurtosis of particle number distributions at r th multiplicity. The corresponding weight for the r th multiplicity is $\omega_r = n_r / \sum_r n_r$.

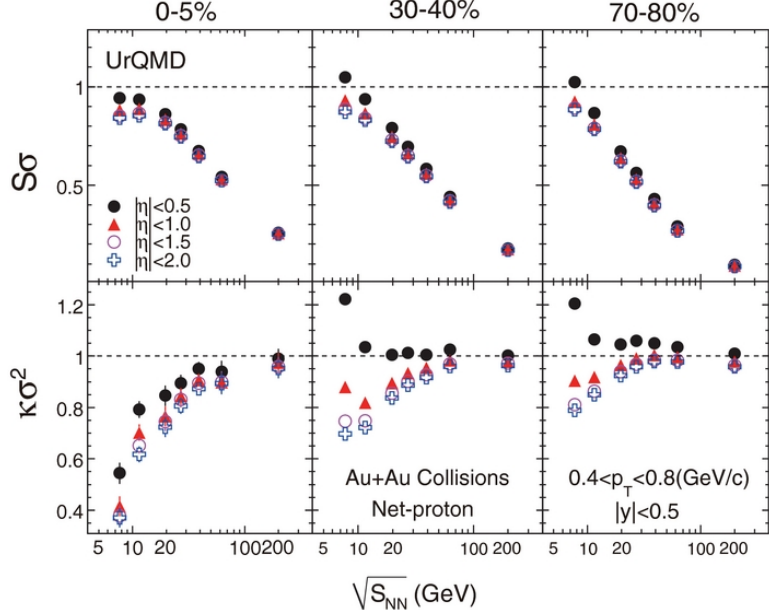


Figure 15: The energy dependence of the moments products ($S\sigma, \kappa\sigma^2$) of net-proton multiplicity distributions for Au+Au collisions at $\sqrt{s_{NN}} = 7.7, 11.5, 19.6, 27, 39, 62.4, 200$ GeV in the UrQMD model with different centrality definitions.

6.2 The centrality resolution effect (CRE)

Particle multiplicity not only depends on physics-based processes, but also reflects the initial geometry of the heavy- ion collision. This indicates that the relation between measured particle multiplicity and the impact parameter does not correspond one-to-one, and there are fluctuations in the particle multiplicity even for a fixed impact parameter. Thus, it could have different initial collision geometry resolutions (centrality resolutions) for different centrality definitions with particle multiplicity.

Figure 15 shows the energy dependence of moment product ($S\sigma, \kappa\sigma^2$) of net-proton multiplicity distributions for three different centralities (0-5%, 30-40%, 70-80%) with four different *eta* ranges in Au+Au collisions. We can find that the $\kappa\sigma^2$ (fourth order fluctuation) is more sensitive to the CRE than the $S\sigma$ (third order fluctuation), and it has a greater effect in the peripheral collision and at low energies. Thus, we should use a larger η range in the centrality definition for the real experimental moment analysis.

7 Efficiency correction and statistical error estimation

In real case, as we don't have 100% detector efficiency (include acceptance), we have to estimate the effect of the detector efficiency on the observable. Generally, the efficiency ε for particle detection can be treated as a binomial sampling $B(\varepsilon, N)$ with a efficiency parameter ε .

Figure 16 and 17 show the p_T dependence of the TPC embedding efficiencies for π, K, p at Au+Au 39GeV. The TPC tracking efficiencies can be estimated by embedding Monte Carlo (MC) tracks in the real event, it can be expressed by: $\varepsilon = N_{rec}/N_{primary}$. The lines in the Figure 16 and 17 are fitted by the function:

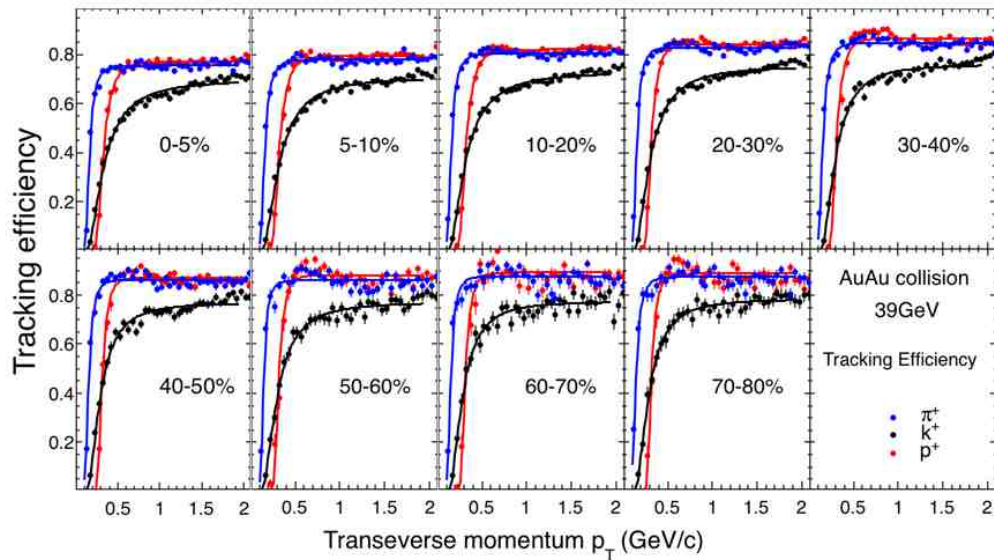


Figure 16: TPC tracking efficiencies for π^+, K^+, p at Au+Au 39GeV.

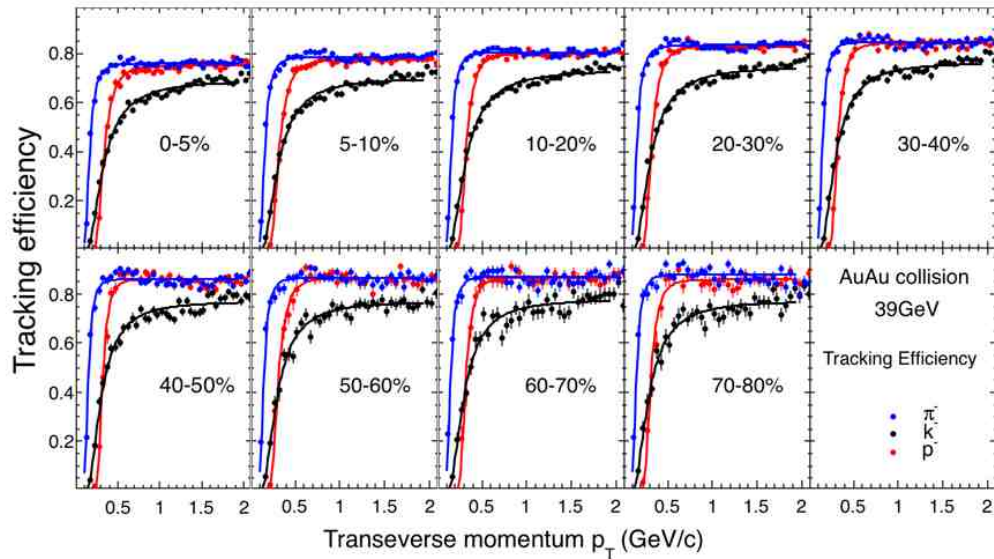


Figure 17: TPC tracking efficiencies for π^-, K^-, \bar{p} at Au+Au 39GeV.

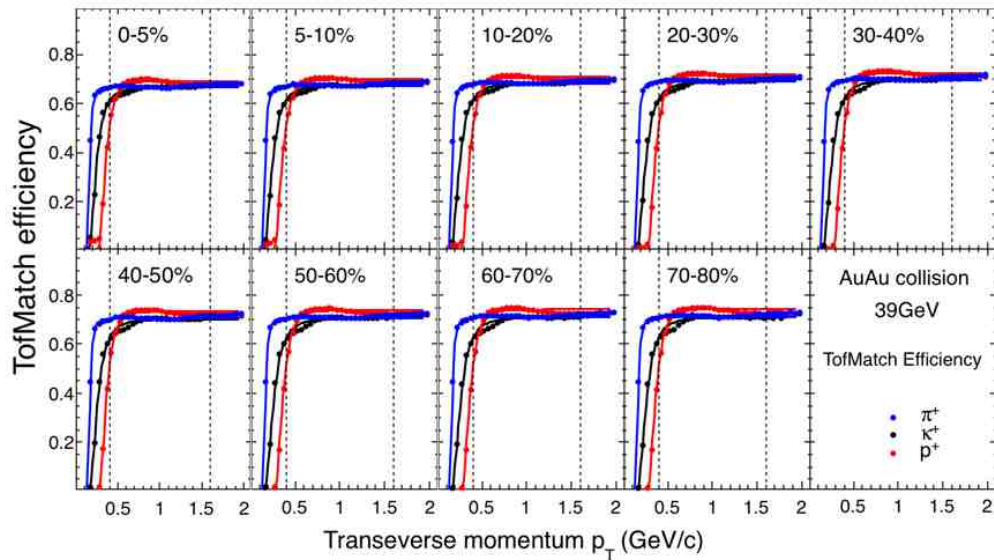


Figure 18: TOF match efficiencies for π^+, K^+, p at Au+Au 39GeV.

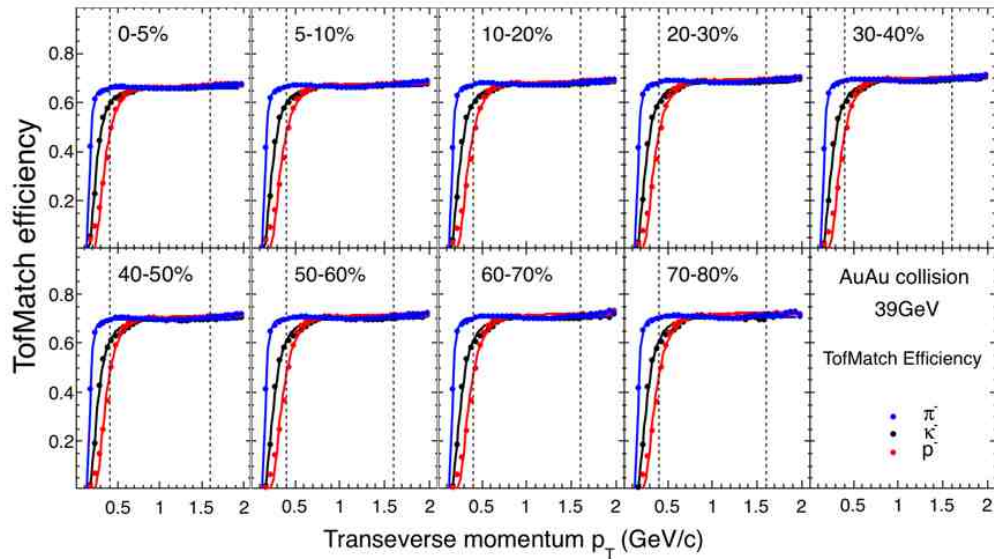


Figure 19: TOF match efficiencies for π^-, K^-, p at Au+Au 39GeV.

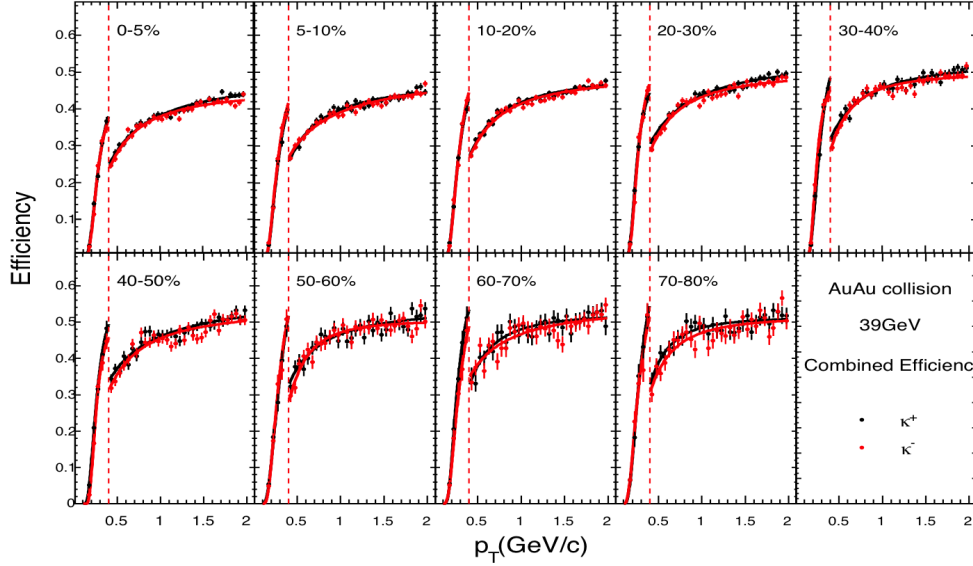


Figure 20: Combined efficiencies for K^+, K^- at Au+Au 39GeV.

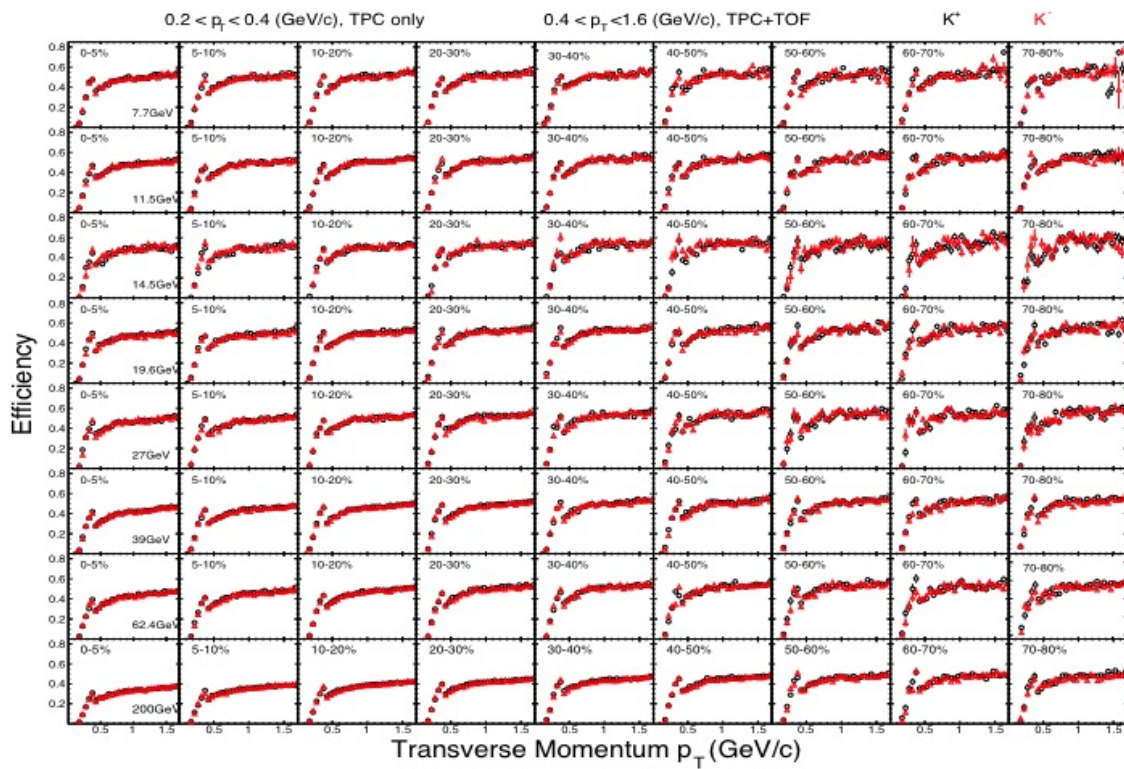


Figure 21: Combined efficiencies for K^+, K^- at Au+Au 39GeV.

$$y = p_0 e^{-(\frac{p_1}{x})^{p_2}} \quad (15)$$

Figure 18 and 19 show the p_T dependence of the TOF match efficiencies for π, K, p at Au+Au 39GeV. It can be expressed by: $\varepsilon = \frac{\int_{N(|n\sigma_{de}/dx| < 0.5 \& \& \beta > 0)}^{} f(p_T) dp_T}{\int_{N(|n\sigma| < 0.5)}^{} f(p_T) dp_T}$. The fit function is same with TPC.

Figure 20 show the centrality dependence of final combined efficiency of TPC and TOF at Au+Au 39GeV. Figure 21 shows all efficiencies of the BESI energies.

The efficiencies in our final calculation is p_T averaged efficiencies and can be calculated based on:

$$\varepsilon = \frac{\int_a^b \varepsilon'(p_T) f(p_T) p_T dp_T}{\int_a^b f(p_T) p_T dp_T} \quad (16)$$

, where the transverse momentum dependence efficiency $\varepsilon'(p_T)$ is from the embedding data with the same track cuts as used in the data analysis. $f(p_T)$ is the efficiency corrected transverse momentum spectra for kaon/anti-kaon. (a, b) is the momentum range. At lower p_T range $0.2 < p_T < 0.4(GeV/c)$, only TPC is used, and at higher p_T range $0.4 < p_T < 1.6(GeV/c)$, both TPC and TOF are used. So the final efficiencies can be calculated by:

$$<\varepsilon_{high}> = \frac{\int_{0.4}^{1.6} \varepsilon_{TPC}(p_T) f(p_T) p_T dp_T}{\int_{0.4}^{1.6} f(p_T) p_T dp_T} \quad (17)$$

$$<\varepsilon_{low}> = \frac{\int_{0.2}^{0.4} \varepsilon_{TPC}(p_T) \varepsilon_{TOF}(p_T) f(p_T) p_T dp_T}{\int_{0.2}^{0.4} f(p_T) p_T dp_T} \quad (18)$$

The efficiencies values in the final correction can be found here. Once we have all the efficiencies, the efficiency correction can be done. We can express the moments and cumulants in terms of the factorial moments, which can be easily efficiency corrected. One can found the details about the efficiency correction in [15, 16, 20]

$$F_{\mu,\nu,j,\kappa}(N_{K_1}, N_{K_2}, N_{\bar{K}_1}, N_{\bar{K}_2}) = \frac{f_{\mu,\nu,j,\kappa}(n_{K_1}, n_{K_2}, n_{\bar{K}_1}, n_{\bar{K}_2})}{(\varepsilon_{K_1})^\mu (\varepsilon_{K_2})^\nu (\varepsilon_{\bar{K}_1})^j (\varepsilon_{\bar{K}_2})^\kappa} \quad (19)$$

The statistical errors are based on Delta Theorem. The Delta theorem is a well known theorem in statistics, which is used to approximate the distribution of a transformation of a statistic in large samples if we can approximate the distribution of the statistic itself. Distributions of transformations of a statistic are of great importance in applications. The details about the error estimation can be found in [16, 17]

8 Systematic error estimation

For the systematic uncertainties estimation, following quality cuts have been used to extract the systematic errors:

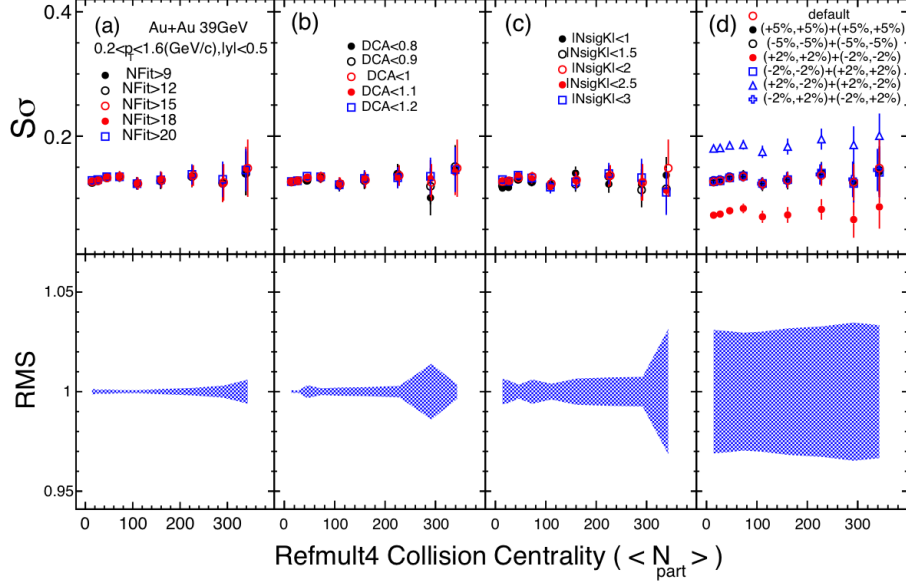


Figure 22: Systematic errors estimation of $S\sigma$ for different cuts at Au+Au 39GeV.

- NFitPoint: 9, 12, 15(default), 18, 20
- DCA: 0.8, 0.9, 1.0(default), 1.1, 1.2
- $n\sigma_K$: 1, 1.5, 2, 2.5, 3
- Efficiency: (K^+ : lower p_T , higher p_T) + (K^- : lower p_T , higher p_T)
 - (+5%, +5%) + (+5%, +5%)
 - (-5%, -5%) + (-5%, -5%)
 - (+2%, -2%) + (+2%, -2%)
 - (-2%, +2%) + (-2%, +2%)

The results from each set of the cuts are corrected for efficiency. For each set of the cuts, we can calculate the point by point difference between the efficiency corrected results from the varied cuts and the default cuts. Then the systematic errors is the sum square root of those difference.

$$RMS = \sqrt{\frac{1}{N} \sum_{i=1}^N (X_i - Y)^2} \quad (20)$$

$$SysErr. = \sqrt{\sum_j RMS_j^2} \quad (21)$$

Figure 22 and 23 show centrality dependence of the efficiency corrected $S\sigma$ and $\kappa\sigma^2$ for variation of track cuts and systematic error in Au+Au collisions $\sqrt{s_{NN}} = 39\text{GeV}$.

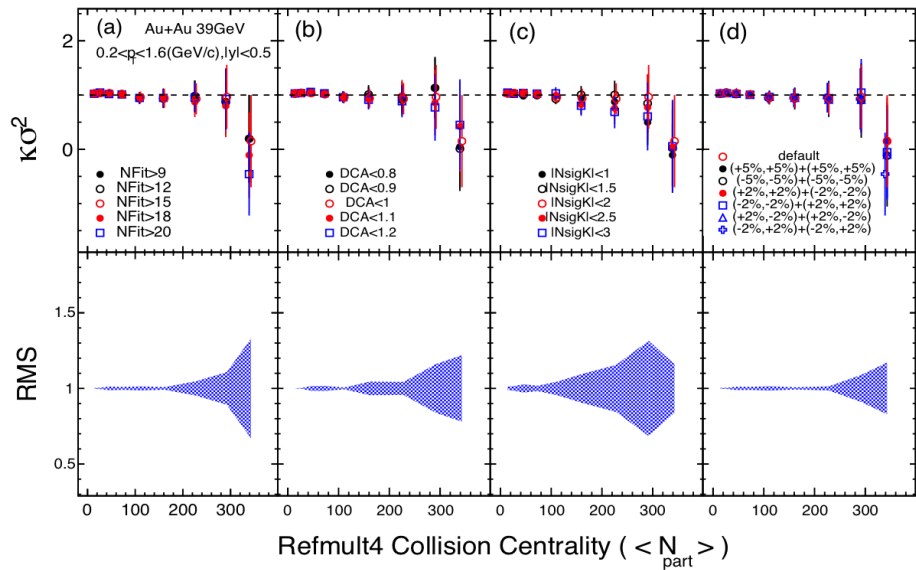


Figure 23: Systematic errors estimation of $\kappa\sigma^2$ for different cuts at Au+Au 39GeV.

9 Baselines for the higher moments

9.1 Poission expectation

Assuming kaon and anti-kaon are independent distributed as Poisson distribution. The difference of two independent Poisson distributions distributed as the Skellam distributions. It's probability density formula is:

$$P(N) = \left(\frac{\mu_1}{\mu_2}\right)^{(N/2)} I_N(2\sqrt{\mu_1\mu_2}) e^{-(\mu_1+\mu_2)} \quad (22)$$

, where the μ_1 and μ_2 are the mean value of two Poisson distributions, respectively, the $I_k(z)$ is the modified bessel function of the first kind. Then the net-kaon distribution can be expressed as skellam distribution. Then the expectation of the various cumulants (C_1, C_2, C_3, C_4) and moment products ($\sigma^2/M, S\sigma, \kappa\sigma^2$) can be written by:

$$C_{2n} = \mu_K + \mu_{\bar{K}}, (n = 1, 2, 3, \dots) \quad (23)$$

$$C_{2n-1} = \mu_K - \mu_{\bar{K}}, (n = 1, 2, 3, \dots) \quad (24)$$

$$\sigma^2/M = \frac{\mu_K + \mu_{\bar{K}}}{\mu_K - \mu_{\bar{K}}} \quad (25)$$

$$S\sigma = \frac{\mu_K - \mu_{\bar{K}}}{\mu_K + \mu_{\bar{K}}} \quad (26)$$

$$\kappa\sigma^2 = 1 \quad (27)$$

, where the μ_K is the mean value of kaon distribution, and the $\mu_{\bar{K}}$ is the mean value of anti-kaon distribution.

9.2 Negative Binomial Distribution

Binomial Distribution (BD) and Negative Binomial Distribution (NBD) are widely used to describe distributions with variance smaller than mean and larger than mean, respectively. Negative Binomial Distribution (NBD) can be expressed as:

$$NB(k; r, p) = \binom{k=r-1}{k} p^r (1-p)^k \quad (28)$$

The cumulants for BD and NBD are:

$$C_2 = \sigma^2 = r\mu \quad (29)$$

$$C_3 = S\sigma^3 = r\mu(2r-1) \quad (30)$$

$$C_4 = \kappa\sigma^4 = r\mu(6r^2 - 6r + 1) \quad (31)$$

, where μ is the mean value, $r = \frac{\sigma^2}{\mu} = 1 - \varepsilon < 1$ is the ratio between variance and mean value. If we assume the kaon and anti-kaon are independent distributed. Then we can obtain the cumulants of net-kaon distributions:

$$C_n = C_n^+ + (-1)^n C_n^- \quad (32)$$

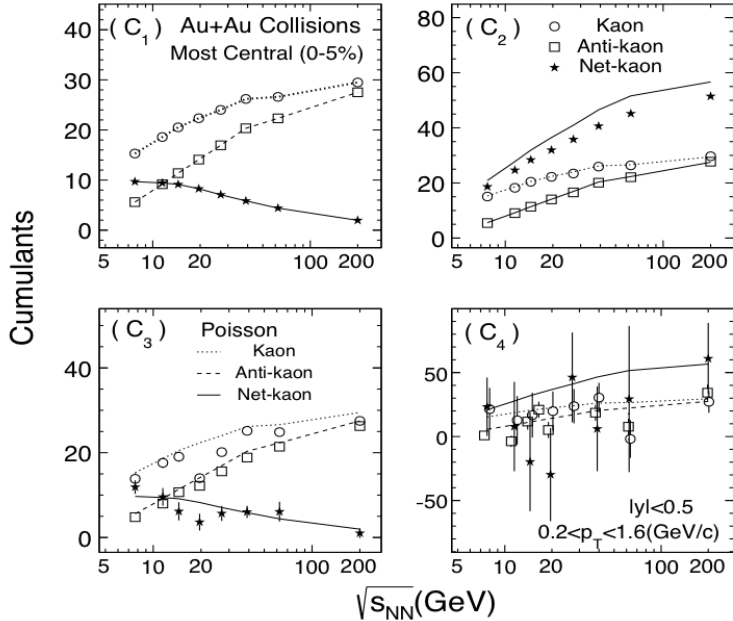


Figure 24: Energy dependence of cumulants of kaon, anti-kaon, and net-kaon multiplicity distributions for Au+Au collisions at $\sqrt{s_{NN}} = 7.7, 11.5, 14.5, 19.6, 27, 39, 62.4$, and 200 GeV for most central(0-5%). The lines are from Poisson expectations. The results are corrected for the kaon reconstruction efficiency.

9.3 UrQMD simulation

The Ultra Relativistic Quantum Molecular Dynamics (UrQMD) is a microscopic many-body approach to study p + p, p + A, and A + A interactions at relativistic energies and is based on the covariant propagation of color strings, constituent quarks, and diquarks accompanied by mesonic and baryonic degrees of freedom. Furthermore it includes rescattering of particles, the excitation and fragmentation of color strings, and the formation and decay of hadronic resonances. UrQMD is a transport model for simulating heavy-ion collisions in the energy range from SIS to RHIC (even in LHC). It combines different reaction mechanism, and can provide theoretical simulated results of various experimental observables. It provides us the baselines and qualitative estimate on the background effects for the experimental search for the QCD phase transition and QCD critical point.

10 Results

The results presented here are obtained from the Au+Au collisions at 7.7, 11.5, 14.5, 19.6, 27, 39, 62.4 and 200 GeV in the first phase of the BES program at RHIC. Energy loss (dE/dx) in Time Projection Chamber and mass-squared (m^2) from Time of Flight are used to identify kaons within $0.2 < p_T < 1.6 \text{ (GeV}/c)$ and at mid-rapidity $|y| < 0.5$. The centrality is determined from the uncorrected charge particle multiplicity by excluding the kaons and anti-kaons within pseudo-rapidity $|\eta| < 1$.

The centrality dependence of cumulants (C_1, C_2, C_3 , and C_4) plotted as a function of N_{part} is presented in Figure 26. The centrality dependence of moment products (σ^2/M , $S\sigma/\text{Skellam}$, and $\kappa\sigma^2$) plotted as a function of N_{part} is presented in Figure 27, 28, and 29, respectively. The

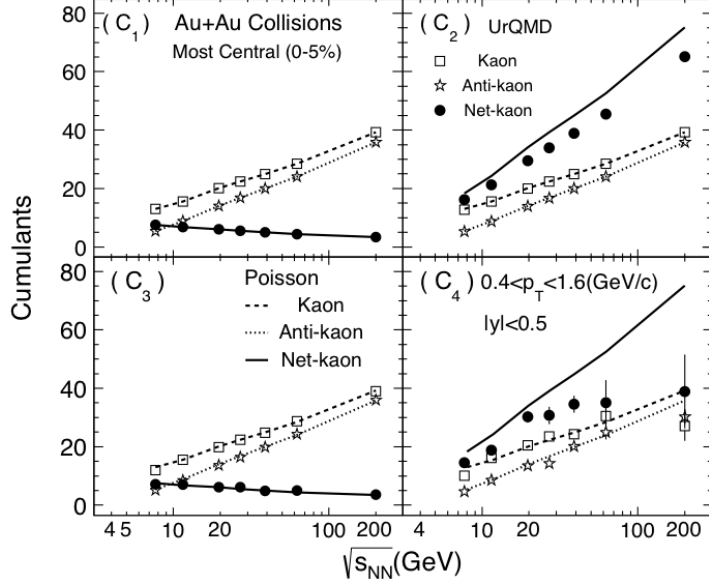


Figure 25: Energy dependence of cumulants of kaon, anti-kaon, and net-kaon multiplicity distributions for Au+Au collisions at $\sqrt{s_{NN}} = 7.7, 11.5, 19.6, 27, 39, 62.4$, and 200GeV for most central(0-5%). The lines represent the Poisson expectations.

results are corrected for the finite centrality bin width effects . We use the Delta theorem approach to obtain statistical errors.

The energy dependence of moment products (σ^2/M , $S\sigma/\text{Skellam}$, and $\kappa\sigma^2$) for two centrality (0 – 5% and 70 – 80%) are presented in figure 30. The Poisson expectations are denoted as dotted lines, the negative binomial distribution baseline are denoted as solid lines, and UrQMD calculations are shown as blue bands. The error bars are statistical and caps are systematic errors. We can see that the values of σ^2/M increase as the energy increases. The values of $S\sigma/\text{Skellam}$ are consistent with poisson and negative binomial distribution baseline within uncertainties. The values of $\kappa\sigma^2$ are consistent with poisson and negative binomial distribution baseline within uncertainties. UrQMD (no Critical Point), shows no energy dependence for $S\sigma/\text{Skellam}$ and $\kappa\sigma^2$.

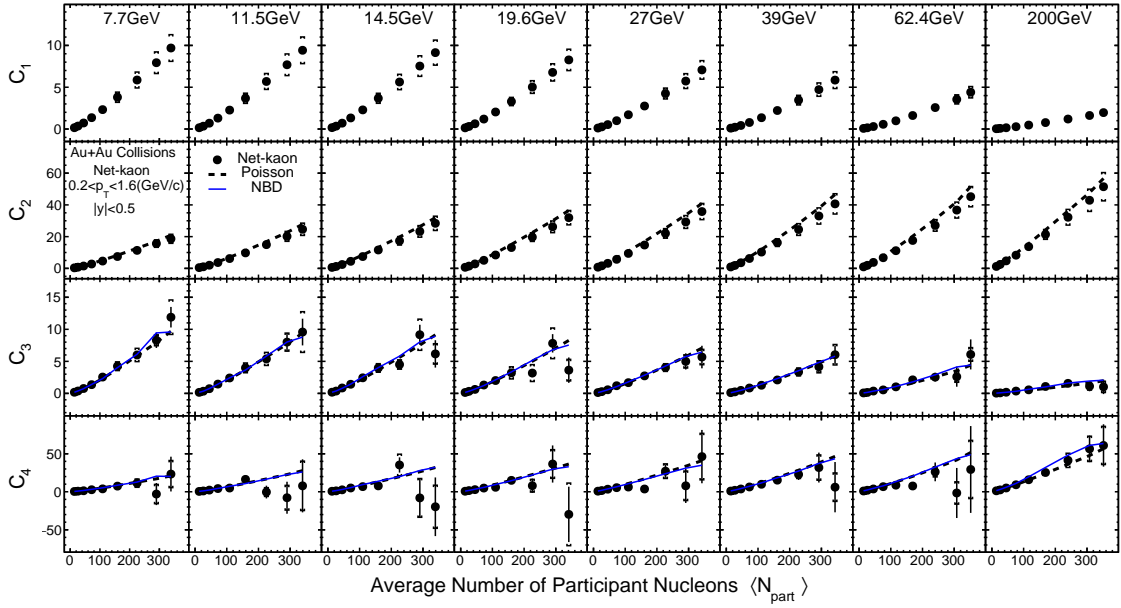


Figure 26: Centrality dependence of cumulants for net-kaon multiplicity distributions in Au+Au collisions at $\sqrt{s_{NN}} = 7.7, 11.5, 19.6, 27, 39, 62.4$, and 200GeV. The results are corrected for the kaon reconstruction efficiency.

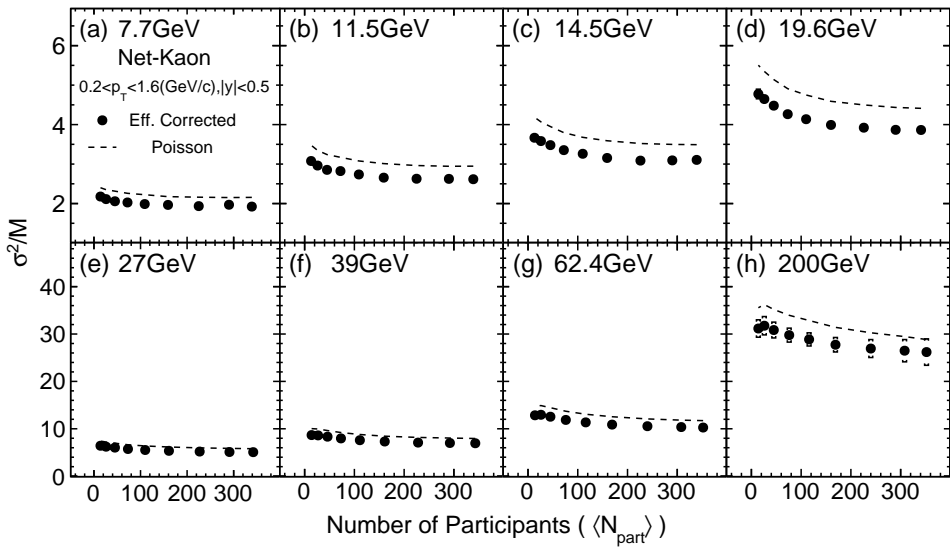


Figure 27: Centrality dependence of σ^2/M for net-kaon multiplicity distributions in Au+Au collisions at $\sqrt{s_{NN}} = 7.7, 11.5, 14.5, 19.6, 27, 39, 62.4$, and 200GeV. The results are corrected for the kaon reconstruction efficiency.

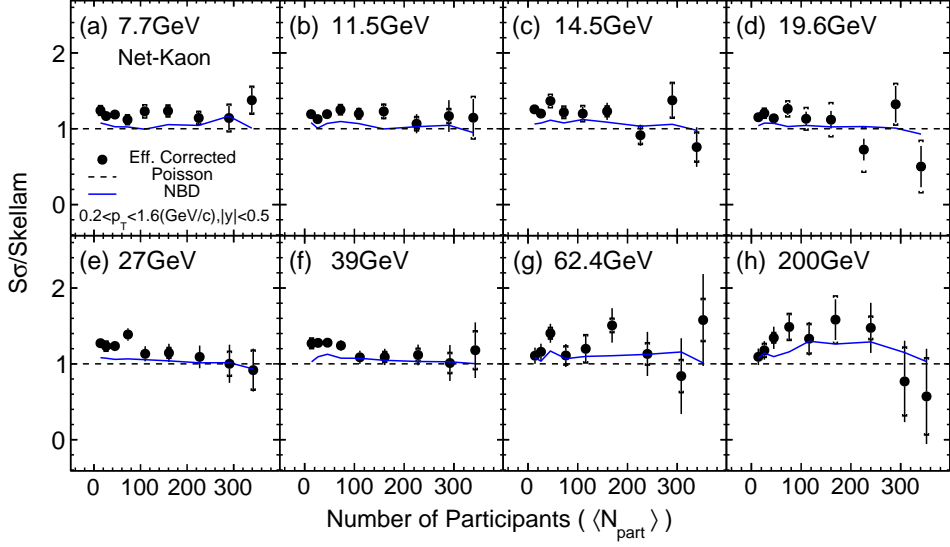


Figure 28: Centrality dependence of $S\sigma/\text{Skellam}$ for net-kaon multiplicity distributions in Au+Au collisions at $\sqrt{s_{NN}} = 7.7, 11.5, 14.5, 19.6, 27, 39, 62.4$, and 200 GeV. The results are corrected for the kaon reconstruction efficiency.

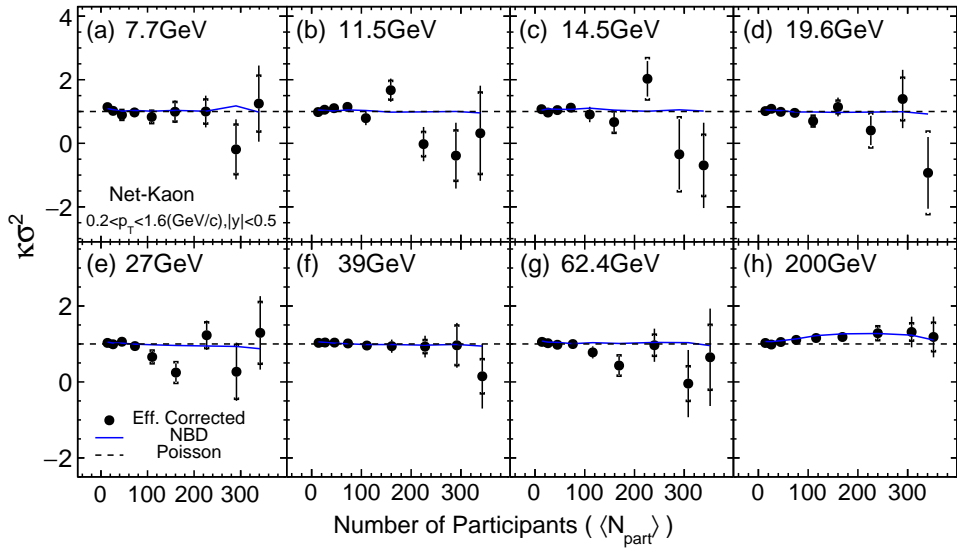


Figure 29: Centrality dependence of $\kappa\sigma^2$ for net-kaon multiplicity distributions in Au+Au collisions at $\sqrt{s_{NN}} = 7.7, 11.5, 14.5, 19.6, 27, 39, 62.4$, and 200 GeV. The results are corrected for the kaon reconstruction efficiency.

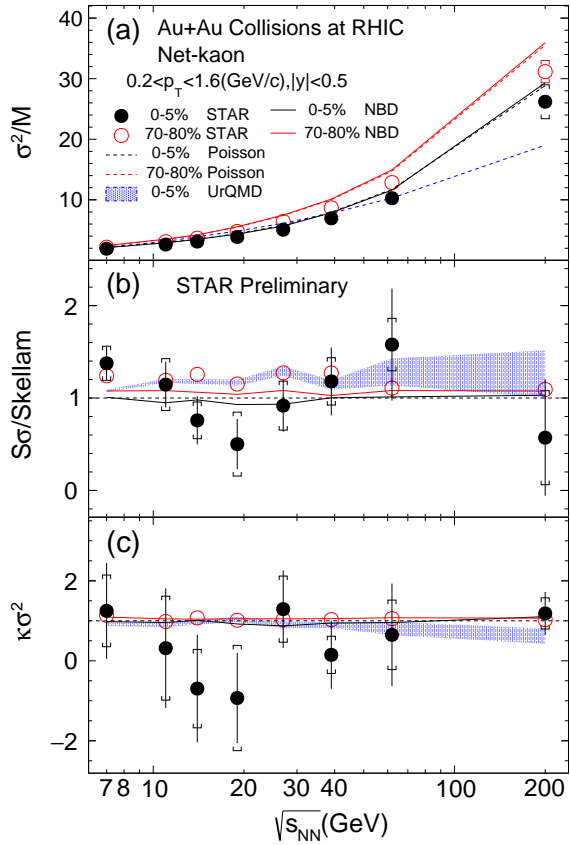


Figure 30: Energy dependence of cumulant ratios (σ^2/M , $S\sigma/\text{Skellam}$, and $\kappa\sigma^2$) for net-kaon multiplicity distributions in Au+Au collisions at $\sqrt{s_{NN}} = 7.7, 11.5, 14.5, 19.6, 27, 39, 62.4$, and 200 GeV. The Poisson expectations are denoted as dotted lines and UrQMD calculations are shown as blue bands. The error bars are statistical and caps are systematic errors.

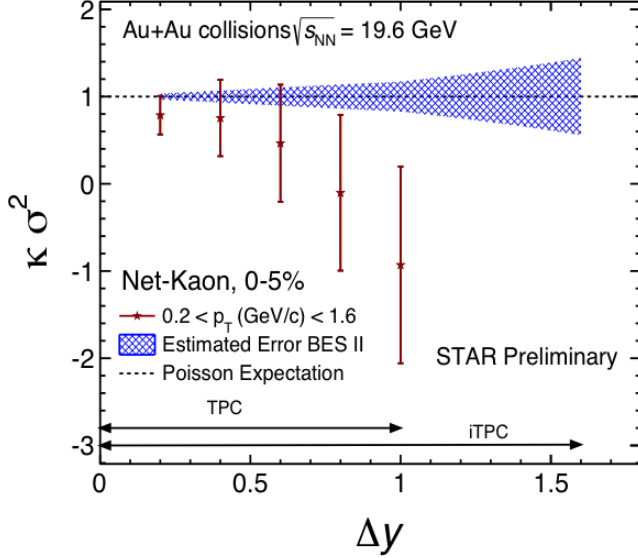


Figure 31: Error estimation (blue band) for net-kaon $\kappa\sigma^2$ in Au+Au collisions at $\sqrt{s_{NN}} = 7.7$ GeV with the upgraded STAR detector and larger statistics in the upcoming RHIC Beam Energy Scan II for an increasing rapidity coverage.

11 Summary and Outlook

- STAR results on collision energy and centrality dependence of net-Kaon cumulants and their ratios, within the kinematic range $[|y| < 0.5, 0.2 < p_T < 1.6 \text{ (GeV/c)}]$, for Au+Au collisions at $\sqrt{s_{NN}} = 7.7, 11.5, 14.5, 19.6, 27, 39, 62.4$ and 200 GeV are presented.
- The values of net-Kaon's $\kappa\sigma^2$ and $S\sigma/\text{Skellam}$ are consistent with poisson and negative binomial distribution baseline within errors.
- Moments results from UrQMD (no Critical Point), shows no energy dependence for $S\sigma/\text{Skellam}$ and $\kappa\sigma^2$.
- The upcoming RHIC BES II in 2019-2020, will include an upgraded STAR detector. An i(nner)TPC and Endcap TOF upgrade will enlarge the phase-space up to $|\eta| < 1.5$ and down to $p_T = 60$ MeV/c. The Event-Plane Detector at forward rapidities will allow for a better centrality estimation, suppressing auto-correlations.

References

- [1] M. A. Stephanov, [Phys. Rev. Lett.](#) **102**, 032301 (2009).
- [2] M. Asakawa, S. Ejiri, and M. Kitazawa, [Phys. Rev. Lett.](#) **103**, 262301 (2009).
- [3] M. A. Stephanov, [Phys. Rev. Lett.](#) **107**, 052301 (2011).
- [4] R. V. Gavai and S. Gupta, [Phys. Rev. D](#) **78**, 114503 (2008).
- [5] M. Cheng, P. Hegde, C. Jung, F. Karsch, O. Kaczmarek, E. Laermann, R. D. Mawhinney, C. Miao, P. Petreczky, C. Schmidt, and W. Soeldner, [Phys. Rev. D](#) **79**, 074505 (2009).
- [6] F. Karsch and K. Redlich, [Physics Letters B](#) **695**, 136 (2011).
- [7] P. Garg, D. K. Mishra, P. K. Netrakanti, B. Mohanty, A. K. Mohanty, B. K. Singh, and N. Xu, [Physics Letters B](#) **726**, 691 (2013).
- [8] J. Cleymans, H. Oeschler, K. Redlich, and S. Wheaton, [Physical Review C](#) **73**, 034905 (2006).
- [9] K. H. Ackermann *et al.* (STAR), [Nucl. Instrum. Meth.](#) **A499**, 624 (2003).
- [10] M. Anderson *et al.*, [Nucl. Instrum. Meth.](#) **A499**, 659 (2003), arXiv:nucl-ex/0301015 [nucl-ex]
- .
- [11] W. J. Llope, *18th International Conference on the Application of Accelerators in Research and Industry (CAARI 2004) Fort Worth, Texas, October 10-15, 2004*, [Nucl. Instrum. Meth.](#) **B241**, 306 (2005).
- [12] X. Dong, *Nuclear physics trends. Proceedings, 6th China-Japan Joint Nuclear Physics Symposium, Shanghai, China, May 16-20, 2006*, [AIP Conf. Proc.](#) **865**, 332 (2006), [,332(2006)].
- [13] H. Bichsel, [Nucl. Instrum. Meth.](#) **A562**, 154 (2006).
- [14] M. L. Miller, K. Reygers, S. J. Sanders, and P. Steinberg, [Annual Review of Nuclear and Particle Science](#) **57**, 205 (2007).
- [15] A. Bzdak and V. Koch, [Physical Review C](#) **91**, 027901 (2015).
- [16] X. Luo, [Physical Review C](#) **91**, 034907 (2015).
- [17] X. Luo, J. Xu, B. Mohanty, and N. Xu, [Journal of Physics G: Nuclear and Particle Physics](#) **40**, 105104 (2013).
- [18] X. Luo and the STAR Collaboration, [Journal of Physics: Conference Series](#) **316**, 012003 (2011).
- [19] V. Skokov, B. Friman, and K. Redlich, [Physical Review C](#) **88**, 034911 (2013).
- [20] A. Bzdak and V. Koch, [Physical Review C](#) **86**, 044904 (2012).